Materials Today Chemistry 44 (2025) 102586

Contents lists available at ScienceDirect

Materials Today Chemistry

journal homepage: www.journals.elsevier.com/materials-today-chemistry/

Sustainable development of dual–templating molecularly imprinted polymers for biopurification

Ana I. Furtado [a,b], Diogo Lobato [a], Vasco D.B. Bonifácio [b,c,*], Raquel Viveiros [a,**], Teresa Casimiro [a,***]

[a] LAQV–REQUIMTE, Chemistry Department, NOVA School of Science & Technology, NOVA University of Lisbon, Campus de Caparica, Caparica, 2829–516, Portugal
[b] iBB–Institute for Bioengineering and Biosciences and i4HB–Institute for Health and Bioeconomy, Instituto Superior Técnico, University of Lisbon, Av. Rovisco Pais, 1, Lisboa, 1049–001, Portugal
[c] Bioengineering Department, Instituto Superior Técnico, University of Lisbon, Av. Rovisco Pais, Lisboa, 1049–001, Portugal

ARTICLE INFO

Keywords:
Synthetic affinity materials
Molecularly imprinted polymers
Dual–templating
Supercritical carbon dioxide
Solid–phase extraction
Biorecognition
Bioseparation

ABSTRACT

The demand for bio–based products is increasing, but the development of efficient purification processes is lagging. However, typically these processes are expensive, non–specific and/or lack of efficiency. Molecularly imprinted polymers (MIPs) are synthetic affinity materials able to mimic the molecular recognition ability of natural molecules, offering a cost–effective alternative to replace the commercial affinity–driven materials based on proteins and antibodies. In this work, MIPs were developed using supercritical carbon dioxide ($scCO_2$) technology using two approaches: i) one–templating (O–MIPs), using L–leucine (LEU) as template, and ii) a dual–templating (D–MIPs), using LEU and L–lysine (LYS) as templates, to evaluate their potential in the molecular recognition of amino acids in simple and complex aqueous solutions. MIPs produced in $scCO_2$ have already shown good performances in organic and aqueous solutions, for small and non–polar template molecules. Herein, their applicability is extended to amino acids but also proteins. MIPs were produced using 2–vinylpyridine (VP) as functional monomer and ethylene glycol dimethacrylate (EGDMA) as crosslinker under $scCO_2$ conditions. Polymers were obtained as white, ready–to–use dry powders. Their affinity performance was assessed by Static Binding Tests (SBTs) and Solid Phase Extraction (SPE) assays using different amino acids and proteins. The best SBT results was obtained by D–MIP with $Q_{max} = 216$ mg LEU + LYS/g D–MIP, and $IF_{max} = 8.3$. D–MIP also presented higher binding capacities to adsorb their templated–molecules by a dynamic process (SPE) ($Q_{max} = 79$ mg LEU + LYS/g D–MIP), and selectively bind their templates in a solution containing a protein ($IF_{max} = 6.8$). The green D–MIP provides a robust, tailor–made and sustainable alternative for biopurification processes.

1. Introduction

The demand of biological–based products is increasing which requires the intensification of separation and purification processes [1]. The most common technologies used for the purification of biomolecules are based on chromatography using protein–based resins [2]. To improve these processes, innovative materials and technologies are sought, such as magnetic materials and protein beads, among others. Ligand tagging systems are increasingly preferred over traditional methods [3]. However, these technologies are very expensive, and a high efficiency is hard to achieve, with strong limitations in terms of cost–effectiveness and productivity as well as storage issues [4]. In addition, these technologies demand several analytical steps, and specialized resources (*e.g.*, consumables, equipment, and qualified operators) [3,4]. Currently, there is a challenge to improve the biological function of these protein–based systems without negatively affecting the

* Corresponding author. iBB–Institute for Bioengineering and Biosciences and i4HB–Institute for Health and Bioeconomy, Instituto Superior Técnico, University of Lisbon, Av. Rovisco Pais, 1, Lisboa, 1049–001, Portugal.
** Corresponding author. LAQV-REQUIMTE, Chemistry Department, NOVA School of Science & Technology, NOVA University of Lisbon, Campus de Caparica, Caparica, 2829-516, Portugal.
*** Corresponding author. LAQV-REQUIMTE, Chemistry Department, NOVA School of Science & Technology, NOVA University of Lisbon, Campus de Caparica, Caparica, 2829-516, Portugal.
E-mail addresses: vasco.bonifacio@tecnico.ulisboa.pt (V.D.B. Bonifácio), raquel.viveiros@fct.unl.pt (R. Viveiros), teresa.casimiro@fct.unl.pt (T. Casimiro).

https://doi.org/10.1016/j.mtchem.2025.102586
Received 7 November 2024; Received in revised form 21 January 2025; Accepted 6 February 2025
Available online 21 February 2025

protein stability, which is of major importance for its applicability [5].

Molecularly Imprinted Polymers (MIPs) have gained attention as alternative materials since they can mimic the biorecognition process with significant advantages such as, cost–effectiveness, robustness, stability under harsh conditions, long lifetimes, easy storage, also providing binding constants comparable to natural systems [6]. MIPs are synthetic materials with specific affinity sites that are complementary in terms of size, conformation, and functionality to the target molecules for which affinity is required. Conventional MIPs have been explored as adsorbents for solid–phase extraction, stationary phase for liquid chromatography, and as mimics of enzymes [7]. However, large amounts of organic solvents are used in their production, being environmentally disruptive. The replacement of organic solvents by supercritical carbon dioxide ($scCO_2$) provides a greener and scalable alternative in MIPs synthesis, with potential application in industry [8,9]. $ScCO_2$ is non–toxic, non–flammable, inert, odorless, can be easily removed without any additional energy input, and can be recycled decreasing the processes costs and making it a scalable green alternative solvent. In addition, $scCO_2$ is aprotic and has high mass transfer and diffusivity, which is not easily achievable when organic solvents are used [10].

The development of MIPs towards one–template (O–MIPs) and using $scCO_2$ as a porogenic agent has already been reported for several applications, such as drug delivery, catalysis, switchable sensors and purification devices [10]. Interestingly, MIPs produced by dual–templating (D–MIPs) using conventional strategies were reported to enhance the MIP recognition efficiency compared to O–MIPs [11]. Moreover, research on D–MIPs has been reported in the literature for biosensors and in solid phase extraction (SPE) processes [12–20]. To the best of our knowledge, herein is described for the first time the development of D–MIPs using a dual–templating approach using $scCO_2$ technology. D–MIPs with molecular recognition ability towards two amino acids were produced, and their affinity and selectivity were assessed using different amino acids and a protein, Bovine Serum Albumin (BSA), relevant for biopurification systems where more specific solutions are required.

2. Materials and methods

2.1. Materials

L–Leucine (LEU, >98 %), L–lysine (LYS, ≥98 %), L–arginine (ARG, ≥98 %), 2–vinylpyridine (VP, >97 %), ethylene glycol dimethacrylate (EGDMA, 98 %), ninhydrin (NIN, ≥95 %), Bovine Serum Albumin (BSA, ≥98 %), SupelcleanTM LC–Ph SPE Tube (3 mL), Syringe PP/PE, Corning syringe filters (pore size 0.2 μm) and sodium hydroxide solution (NaOH, 49–51 %) suitable for HPLC, were purchased from Sigma–Aldrich. The solvent ethyl acetate (EtOAc, ≥99.5 %) was purchased from Honeywell. 2,2′–Azobis(2,4–dimethylvaleronitrile) (V–65, 98 %) was purchased from Wako Pure Chemical Industries. SnakeSkin™ Dialysis Tubing was purchased from Thermo Scientific. Carbon Dioxide was obtained from Air Liquide with purity better than 99.998 %. All commercial reagents were used as received. The water used was purified using Millipore Milli–Q lab water system.

2.2. Synthesis of one– and dual–templating molecularly imprinted polymers in $scCO_2$

Amino acids are polar molecules that have low solubility in $scCO_2$. Based on our previous work, EtOAc was used as cosolvent to enhance LEU solubilization in $scCO_2$ [21]. Without the cosolvent, amino acids are not very soluble in $scCO_2$. Preliminary solubility tests were performed using several amino acid solutions (3–6 mg of amino acid/0.5 mL EtOAc) to assess their solubility in $scCO_2$ using a 33 mL high–pressure stainless–steel cell. A maximum concentration of 5.25 mg (LEU + LYS) (equimolar) in 0.5 mL EtOAc was obtained. Therefore, for the syntheses, a maximum of 5.25 mg of the amino acids were used as template(s), previously dissolved in 0.5 mL of EtOAc and kept under stirring for 4 h. The $scCO_2$–assisted MIPs production used a Template(s):Monomer:Crosslinker (T:M:C) molar ratio of 1:50:100, and 2 wt% V–65 as the initiator (relatively to the total weight of monomer and crosslinker). The template solution, VP as functional monomer, EGDMA as crosslinker, and the thermal initiator V–65, were placed in a 33 mL high–pressure cell at 45 °C under stirring for 24 h, and the CO_2 was loaded up to 20 MPa using a Knauer–1900 liquid pump. In the end of the polymerization step, the polymer was subsequently washed with fresh high–pressure CO_2 for 1 h to remove any unreacted reagents. Non–imprinted polymer (NIP) was synthesized following the same procedure, with the exception that no template(s) was added to the cell. Fig. 1 shows the chemical structures of the monomers, and the templates used in our study.

2.3. $ScCO_2$–assisted template desorption

The template desorption was performed packing each pre–synthesized MIP on a stainless–steel tubular column coupled to a 33 mL high–pressure cell containing 3 mL of EtOAc at 40 °C and 20 MPa in continuous flow for 3 h. Both high–pressure cells were immersed in a thermostatted water bath at 40 °C, and CO_2 was bubbled through the cell containing the co–solvent (bottom to top) and the mixture CO_2–EtOAc was passed through the tubular reactor using a Knauer–1900 liquid pump. To evaluate the template desorption efficiency, the following procedure was performed: 20 mg of desorbed MIP was crushed and placed in a vial with 3 mL of milli–Q water and kept under stirring for 24 h. Then, the sample was filtered through a 0.2 μm filter, and quantified by high–pressure ionic chromatograph (HPIC), described in section 2.12. No residues of the amino acid templates were detected by the HPIC analysis (detection limit of 0.5 ppm).

2.4. Scanning electron microscopy (SEM)

All materials were characterized using scanning electron microscopy (SEM) in a Hitachi S–2400 instrument, with an accelerating voltage set to 15 kV. The samples were prepared on aluminum stubs with carbon tape and were gold coated. The magnification used was ×10 000.

2.5. Fourier transform infrared spectroscopy (FTIR–ATR)

The FTIR spectra were acquired for the synthesized materials, using a PerkinElmer Two spectrometer with 16 scans per second and a resolution of 1 cm^{-1}, from 4000 to 400 cm^{-1}.

2.6. Average particle size and particle size distribution

The particle size distribution and the average particle size diameter of the materials were determined using a Morphologi G3 equipment from Malvern. A typical analysis was performed by dispersing the sample using specific conditions: sample volume 13 mm^3, SDU setting (injection pressure: 4 bar, injection time: 40 ms, setting time: 120 s), optic selection 50×. The analysis was performed with at least 30 000 particles, and triplicated samples of each material.

2.7. Zeta potential

Potentiometric measurements were performed on both NIP and MIPs in a Zetasizer Nano ZS from Malvern. The particles were resuspended in distilled water with a concentration of 5 mg/mL, sonicated for 3 min and then transferred to a disposable folded capillary cell. The zeta potential was measured using the supplied Zetasizer software.

2.8. Accelerated surface area and porosimetry (ASAP)

The specific surface area and the average pore size diameter of materials were determined by N_2 adsorption according to the

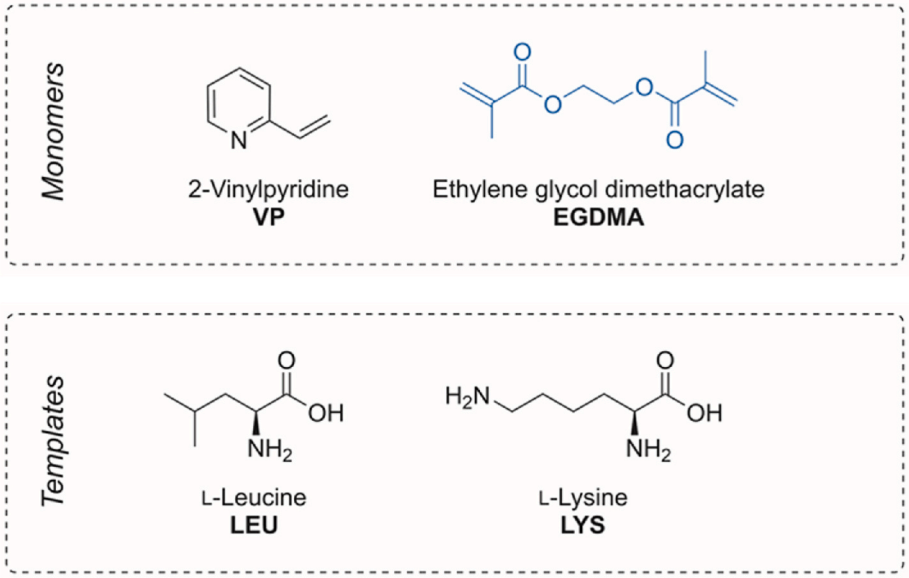

Fig. 1. Chemical structures of the monomer (VP), the crosslinker (EGDMA) and the templates (LEU and LYS).

Brunauer–Emmett–Teller (BET) method. An accelerated surface area and porosimetry system (ASAP 2010 Micromeritics) was used under N_2 flow. The analyses were performed at a temperature of −195.8 °C, and the degasification was performed under vacuum atmosphere until 150 °C for more than 3 h.

2.9. Static binding tests (SBT)

The binding capacity of the materials was evaluated using different amino acids aqueous solutions. For the LEU + LYS MIP, the solutions tested were 0.5 mg/mL of LEU, 0.5 mg/mL of LYS and, 0.5 mg/mL of LEU + LYS (1:1 equimolar), and for the LEU–MIP the template solution of 0.5 mg/mL LEU was tested. All NIPs were tested using the same conditions. The SBTs were performed in triplicated assays. To perform these tests, 20 mg of each material (MIPs and NIP) were weighted and placed into snakeskin dialysis membranes which were then, introduced in 25 mL of template(s) solution, during 24 h under stirring (100 rpm) (IKA KS 4000 I Control shaker with an orbital movement), at room temperature. After this period, 2.5 mL of each solution was analyzed by UV–Vis through the ninhydrin (NIN) colorimetric method. The binding capacity (Q) was determined using Equation (1).

$$\boldsymbol{Q} = \frac{(\boldsymbol{C_0} - \boldsymbol{C})\boldsymbol{V}}{\boldsymbol{W}} \quad (1)$$

where Q is the binding capacity (mg amino acid/g material), C_0 is the biomolecule concentration (mg biomolecule/mL) before sorption, C is the biomolecule concentration (mg biomolecule/mL) in the solutions measured after sorption, V (mL) is the volume of the solution and W (mg) is the sample polymer weight. The imprinting factor (IF), that reflects the MIP binding capacity compared to NIP, was calculated using Equation (2).

$$\boldsymbol{IF} = \frac{\boldsymbol{Q_{MIP}}}{\boldsymbol{Q_{NIP}}} \quad (2)$$

The Q_{MIP} and Q_{NIP} are the binding capacities of the MIP and NIP, respectively.

2.10. Dynamic binding tests

SPE assays were performed to evaluate the dynamic binding performance. Samples of 20 mg of each MIP and NIP were weighed, and packed into blank columns, between two silica plates (Fig. 2). Each SPE experiment involved three steps: conditioning, loading, and washing/elution. In the conditioning phase, 10 mL of milli–Q water was passed twice through the column and collected. Then, in the loading step, 10 mL of an aqueous solution containing the biomolecules (each individual amino acid, a mixture of amino acids – LEU, LYS, ARG – or BSA) was passed one time, collected and analyzed to quantify the amount of adsorbed biomolecules. Finally, the columns were washed (3 cycles), using 10 mL of an EtOAc aqueous solution (10 % v/v) per cycle, to ensure that all biomolecules retained in the loading step were eluted. All samples collected were analyzed by the NIN colorimetric method (amino acids) or by UV–Vis (BSA). The assays were performed in duplicate.

2.11. Amino acids and BSA detection

To determine the amino acids (LEU, LYS and ARG) content present in the samples (SBT and SPE assays), a colorimetric (NIN) method was followed, adapted from literature [22]. A 0.05–0.5 mg/mL concentration range and 1 mL of NIN for 2.5 mL of amino acid solution was used. In a first step, the amino acid solution was homogenized, so the samples were kept under stirring (100 rpm) for 1 min and, NIN was then added, under stirring for one more min. After that, the samples were introduced in a water bath at 50 °C under stirring (approximately 70 rpm) for 10 min. At the end of the procedure, the samples were removed from the water bath and placed in ice bath to stop the derivatization reaction. The samples were analyzed after 5 min using the PerkinElmer Lambda 25 UV–VIS Spectrometer at 565 nm to record the respective absorbance. Solutions of different colors were obtained: purple for LEU and ARG, reddish brown for the LYS and LYS + LEU and pinkish purple for the triple solution (LEU + LYS + ARG). For BSA quantification, a 0.05–0.5 mg/mL concentration range was used and the samples analyzed by UV–Vis. All the calibration curves used in this work are presented in Supplementary Information.

2.12. High pressure ion chromatography (HPIC)

The amino acid solutions with concentrations lower than 0.05 mg/mL, such as for the template desorption efficiency, were analyzed by HPIC. The samples were analyzed using a Dionex ICS3000 equipment with an electrochemical detector – Pulsed Amperometry Detection (PAD), and Aminopac PA10 250×4 mm column with a pre–column of 50×4 mm as the stationary phase, at 30 °C. The mobile phase contained

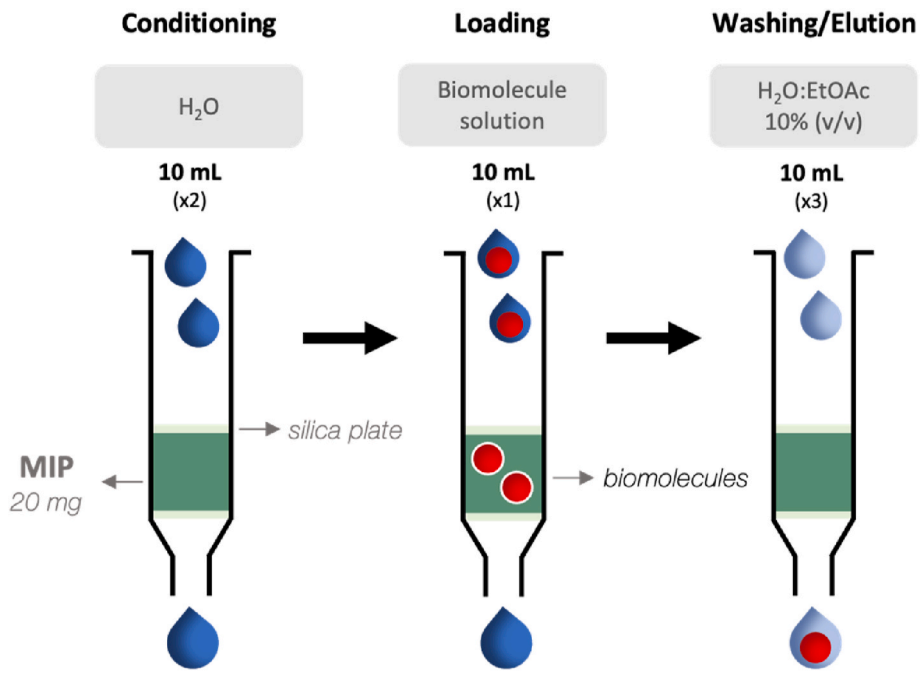

Fig. 2. Schematic protocol for the solid phase extraction (SPE) assays.

a NaOH gradient solution (60–90 mM) at a constant flow of 0.8 mL/min. The injection volume of amino acid samples was 10 μL. The retention time for each amino acid was 2 min for LYS and 12 min for LEU.

3. Results and discussion

All the prepared materials were obtained as white, free flowing, soft dry powders (Fig. 3). The highest yield was achieved for NIP (60 %), while for MIPs the yields were lower than 40 % (Table 1). In the period of 4–6 h, the polymerization was visually followed through the sapphire windows of the high–pressure cell. A single homogeneous phase was initially obtained, meaning that all starting materials were fully dissolved in $scCO_2$. In both MIP systems, a homogeneous phase was only reached after 6 h of reaction, in contrast to the NIP reaction that occurred in a few minutes. For MIPs, after 7 h of reaction, the first polymeric particles began to form, and the polymerization was stopped at 24 h. The observed yield differences for MIPs and NIP could be attributed to amino acids interaction with the growing polymer.

Fig. 3. Dual–templating D–MIPs synthesized in $scCO_2$.

The template(s) desorption from the material was very efficient since no template residues were detected by HPIC analysis (Fig. S1 at Supplementary Information). The average particle size diameter was assessed by Morphologi G3, and the porosimetry properties of the materials (surface area, pore volume and pore size) were obtained by the BET method–ASAP. The ASAP isotherms (type–IV) of the MIPs (Fig. S7 at Supplementary Information) display a hysteresis typical of mesoporous materials [23]. The SEM images of the synthesized materials are presented in Fig. 4.

According to Table 1 and it is evident that template(s) addition in the polymerization significantly affects the material's properties, providing higher particle size diameters and higher porosity for MIPs.

The observed morphology can also be related with the template(s) size used on the MIP systems since higher values of the previous properties were obtained for the D–MIP, in which LYS (146.25 Å) has a higher molecular volume than LEU (134.50 Å) and this might lead to the formation of larger imprinted cavities (Fig. 5) [24]. However, there is no reported evidence that the use of larger templates will result in higher porosity and particle diameters, being these usually attributed to the porogenic agent [11].

The D–MIP, the O–MIP and the respective NIP presented a very similar morphology, where slightly agglomerated spherical polymeric particles are observed. However, in contrast to the average particle size diameter, the NIP agglomerates (Fig. 4c) were larger than in O–MIP (Fig. 4a), while the O–MIP presented larger agglomerates than the D–MIP (Fig. 4b). Therefore, template addition and larger template(s) led to more agglomerated particles (~3 μm) composed by smaller particles (than O–MIP and NIP) with higher pore size (~22 nm). All morphological results were like those reported for precipitation polymerization reactions in $scCO_2$ [21].

Potentiometric measurements revealed different zeta potential values for NIP and MIP particles, with NIP exhibiting a slightly negative

Table 1
Physical properties of the produced materials: D–MIP, O–MIP and NIP.

Polymer	Yield (%)	Average particle size diameter (μm)	Surface area (m^2/g)	Pore volume (cm^3/g)	Pore size (nm)	Surface charge (mV)
O–MIP	26	1.72 ± 0.22	41.97 ± 1.34	0.27 ± 0.01	25.56 ± 0.80	−3.12 ± 0.14
D–MIP	38	2.72 ± 0.25	58.56 ± 2.86	0.34 ± 0.01	22.79 ± 1.13	−2.24 ± 0.16
NIP	60	1.55 ± 0.29	31.26 ± 5.24	0.15 ± 0.01	20.06 ± 3.62	−11.37 ± 0.29

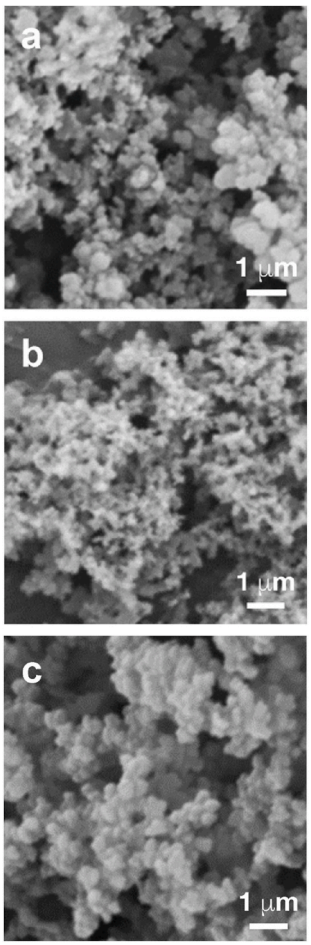

Fig. 4. SEM images obtained for the materials: O–MIP (**a**), D–MIP (**b**) and the corresponding NIP (**c**) (magnification 10000×).

surface charge, while MIPs are considered neutral. This suggests that the introduction of amino acids influences the spatial orientation of the particles, leading to slight differences in charge distribution, attributed to the potentially ionizable pyridines in VP [25]. In the binding tests, a low contribution of ionic interactions between the material and the molecules is expected since MIPs have an almost neutral surface [26, 27].

The FTIR spectra clearly show the characteristic bands of the monomer (VP) and the crosslinker (EGDMA) functional groups (see in Fig. S6 at Supplementary Information).

The D–MIP approach was designed as a new and specific solution for biopurification processes. Therefore, with this aim, the binding performance was evaluated on D–MIP, O–MIP, and NIP using template(s) aqueous solutions. The binding capacities and their respective *IF*s from the static binding tests (SBTs) are presented in Fig. 6. Detailed results of the SBTs are provided in Table S1 in Supplementary Information.

Both MIPs (O–MIP and D–MIP) showed higher binding capacity (Q) over the control material (NIP). Although the NIP has no affinity sites to the amino acids studied, it could also adsorb the amino acid through non–specific interactions. The best binding performance was obtained for the D–MIP, where a Q_{max} of 216 mg LEU/g D–MIP and IF_{max} of 8.3 at 0.5 mg/mL LEU + LYS solution tests were obtained. Comparing the results from the LEU solution test and LYS solution test, performed with the D–MIP, it could be inferred that D–MIP has a higher recognition ability to the LYS at 0.5 mg/mL (static conditions). In general, for all solutions, an *IF* above 1 was obtained (Fig. 6b). This means that the MIP had higher affinity to the amino acids comparing to their correspondent NIP, indicating that a successful imprinting process occurred within the crosslinked materials produced.

These MIPs were designed to be applied as devices for potential use in biopurification processes, which are usually carried out under a dynamic mode. There are several parameters involved in the device performance optimization, such as pressure, temperature, number of cycles and flow rate. SPE is one of the most widely used processes in purification processes in industry [28]. Therefore, SPE lab–scale columns were packed with the produced materials to evaluate their binding performance. All the SPE data results are provided in Supplementary Information, Tables S2–S8.

Initially, the loading step solutions had just one amino acid (LEU or LYS or ARG), to assess the affinity and selectivity of the produced MIPs. The amino acid ARG was chosen for the selectivity assays due to its similarity in size (148.43 $Å^3$) and flexible conformation (5 rotatable bonds) compared to the template molecules [21]. Then, the SPE experiments were performed loading an equimolar solution of two amino acids (LEU and LYS), and an equimolar solution of three amino acids (LEU, LYS and ARG). The results obtained are presented in Fig. 7, and the *IF* values are listed in Table 2.

Then, loading solutions (0.5 mg/mL) of amino acids (LEU and/or LYS) with a model protein, BSA, were evaluated. These SPE experiments aimed to assess the binding performance of the D–MIP in more complex systems (*e.g.*, biomolecules of different sizes), that could be found in bio–industry processes [29]. Therefore, the following biomolecule loading solutions were prepared as well as for its control NIP: (0.25 mg BSA + 0.25 mg LEU)/mL, (0.25 mg BSA + 0.25 mg LYS)/mL, (0.25 mg BSA + 0.125 mg LEU + 0.125 mg LYS)/mL, and 0.25 BSA mg/mL (Fig. 8).

The performance of the SPE experiments was different depending on the solution used, and the MIP packed. The best binding performance was obtained for D–MIP (Fig. 7) (Q_{max} = 79 mg LEU/g D–MIP with LEU solution test and *IF* of 1.6). The D–MIP presented affinity to their templates ($IF > 1$, for LEU solution, LYS solution and LEU + LYS solution) and selectivity ($IF < 1$, for the ARG solution). Otherwise, the performance of the O–MIP in these SPE experiments was not as good as for the D–MIP, indicating its lack of selectivity ($IF = 1$ for both LEU solution and ARG solution), in which it is expected that the number of non–specific interactions between the ARG and O–MIP and between ARG and NIP are higher than between ARG and D–MIP. In general, the D–MIP demonstrates a more robust performance in amino acid mix solutions when compared to O–MIP and NIP. A possible explanation for this observation is the interplay of competitive and cooperative binding among the amino acids, which may result in more favorable configurations of the target molecules within the imprinted microcavities of the D–MIP. However, it must be taken into account the complexity of these biomolecule adsorption phenomena with polymers, for which high–certainty answers are still not available in MIP literature.

Contrary to the SBT, the D–MIP had a better performance with the LEU solution in comparation to the O–MIP, and higher recognition ability to the LEU *vs.* LYS was obtained. On other hand, the O–MIP

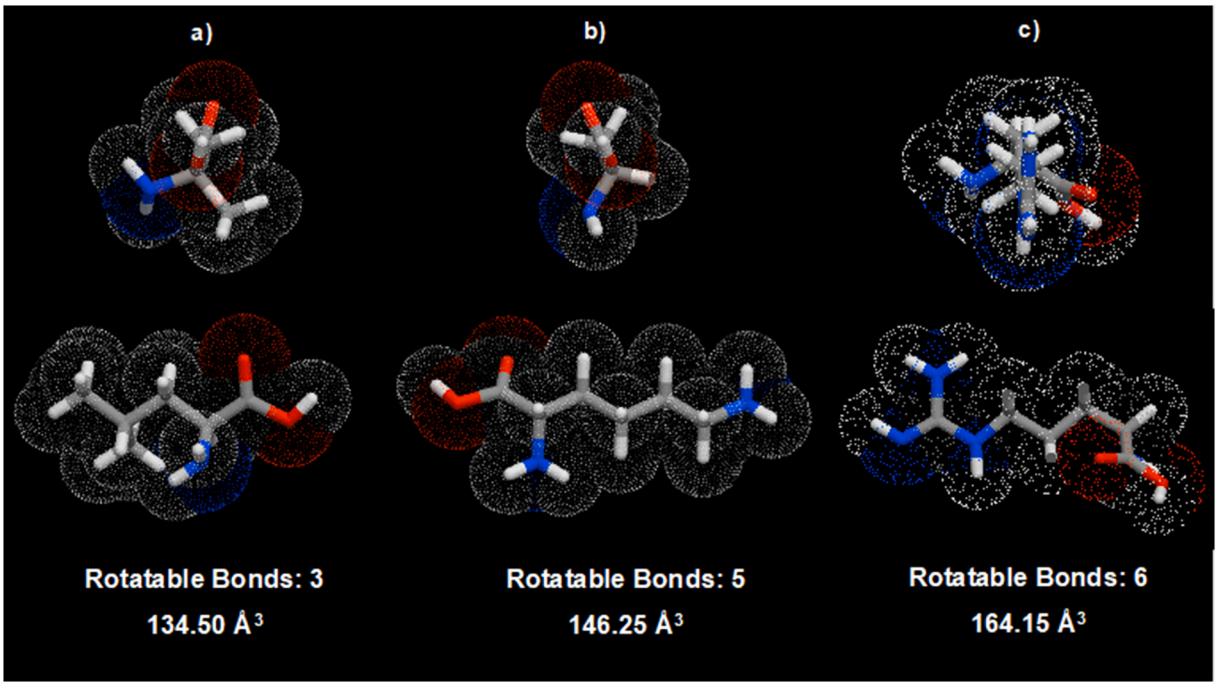

Fig. 5. Spatial conformation, number of rotatable bonds and occupied volume of LEU (**a**), LYS (**b**), and ARG (**c**). Data obtained using the *Molinspiration* software [24].

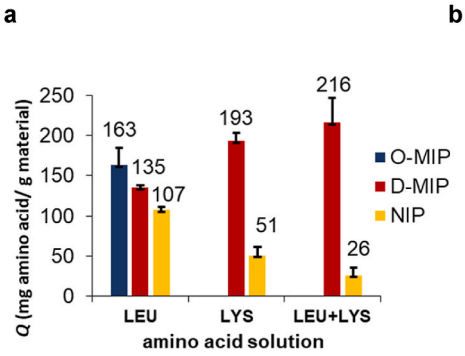

Polymer	LEU	LYS	LEU+LYS
O–MIP	1.7	–	–
D–MIP	1.3	3.8	8.3

Fig. 6. Static binding performance of the produced materials with template(s) solutions: binding capacities (**a**) and imprinting factors (**b**).

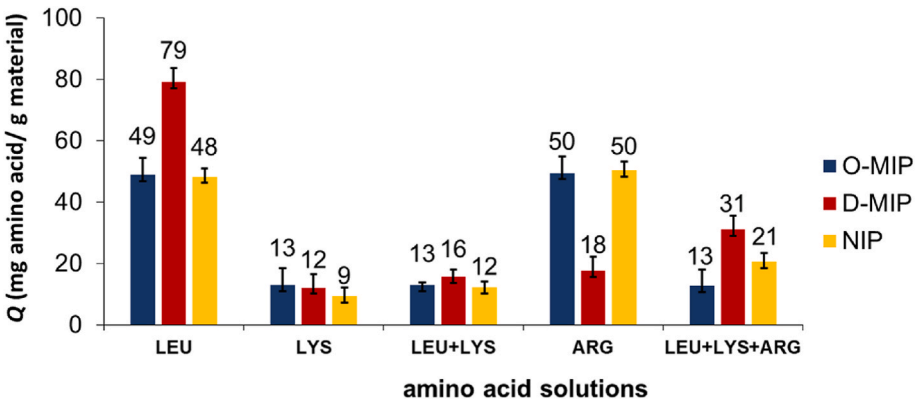

Fig. 7. SPE data for the produced materials obtained using single (LEU, LYS and ARG), and mixed (LEU + LYS and LEU + LYS + ARG) amino acid aqueous solutions (0.5 mg/mL).

showed lower selectivity since higher *IF* values were obtained with the other amino acid solutions rather than with its template solution. In dynamic conditions, such as those present in SPE experiments, factors like the flow rate and contact time between the polymer and target molecules play a significant role in binding performance. LEU, having a smaller molecular volume compared to LYS, can more easily diffuse into and interact with the microcavities of the D–MIP. This enhanced accessibility likely contributes to the higher binding capacity observed

Table 2
Imprinted factor results of the produced materials obtained using single (LEU, LYS and ARG), and mixed (LEU + LYS and LEU + LYS + ARG) amino acid aqueous solutions (0.5 mg/mL).

Polymer	LEU	LYS	LEU + LYS	ARG	LEU + LYS + ARG
O–MIP	1.0	1.4	1.1	1.0	0.6
D–MIP	1.6	1.3	1.3	0.4	1.5

for LEU. Additionally, the dynamic mode may amplify the differences in molecular interactions within the microcavities and polymer morphology, further favoring LEU adsorption. The superior performance of the D–MIP over the O–MIP, namely in the LEU solution, may also be attributed to the larger particle size and higher surface area of the D–MIP. These findings suggest that the interplay between dynamic experimental parameters, molecular volume (size and conformation) and polymer morphology are related to the observed binding behavior.

The SPE experiment for D–MIP with the BSA + LEU solution showed to have the highest binding capacity (Q_{max} = 19.2 mg BSA + LEU/g D–MIP), however the highest amino acid binding capacity was achieved by the D–MIP with BSA + LEU + LYS solution (Q_{max} = 11.6 mg LEU + LYS/g D–MIP, and IF_{max} = 6.8). This can be explained due to the non–specific interactions that occur between the protein and the surface of the polymers [30,31]. Although the D–MIP has no size–protein cavities, it could adsorb the amino acids (*e.g.,* LEU, LYS) present at the surface of the BSA structure within the polymeric structure. Comparing the results between solutions of BSA + LEU and BSA + LYS, the D–MIP seems to have higher ability to anchor BSA protein when the LYS is not in solution, indicating that the LYS imprinted cavities could be responsible for the favorable BSA binding. This could be expected since the molecular volume of LYS is higher than the one of LEU (Fig. 5) and, a higher number of rotatable bonds are found in LYS compared to LEU, which could result in multiconformational LYS cavities and might be more adjustable for amino acids residues present in the protein surface. Therefore, the multiconformational nature of the templates used is a significant factor in the production of D–MIPs. This type of interaction between the LYS molecularly imprinted cavities and proteins has already been reported in the literature [32]. The same behavior could happen with the LEU molecule referring to the LYS and LEU + LYS imprinted cavities, since the LEU has a smaller spatial volume than that of LYS, which could easily fit inside the cavities formed by LYS. For example, this could be reflected in the LEU experiment (Fig. 7) where a higher binding capacity was obtained for the D–MIP when compared to the O–MIP.

The D–MIP had a much better binding performance compared to the NIP, mainly for the amino acid binding capacity, presenting a maximum *IF* of 6.8 for the BSA + LEU + LYS loading solution. In this experiment, the protein binding capacity decreased in both polymers, D–MIP and NIP, which could be related to the fact that both amino acids are smaller than the protein, thus being readily trapped within the polymer matrix leaving no space for the protein to anchor, a common behavior in aqueous phase adsorption processes [33]. Competitive interactions between the amino acids and the protein, and the amino acids with the polymeric matrix could be considered. The interactions of BSA with amino acids have been reported in several studies mainly by aliphatic hydrophobic interactions [34,35]. Based on the results obtained by the D–MIP, the interactions between amino acids and the polymeric matrix are favored, possibly because of the specific interactions occurring within the imprinted cavities. The imprinting effect is particularly notable when both templates are present. In contrast, concerning the NIP, although the amino acid binding capacity is constantly smaller compared to the MIP, a significant decrease of the amino acid binding capacities was observed comparing experiments using protein solutions containing amino acids *versus* experiments using just amino acids. This may also be attributed to preferred interactions between the amino acids and the protein (*e.g.*, hydrophobic interactions and interactions related to the molecule's charge, as discussed further below).

Regarding D–MIP high binding performance, this could be explained based on its morphology, presenting the highest pore volume and surface area, enhancing material diffusivity, and consequently promote the interactions between the target molecules and material, resulting in a high binding performance on the SPE experiments, mainly in the experiments containing BSA. It should also be noted that in the 2nd replicate of the SPE experiment for NIP with only the BSA protein, there was a significant decrease in the binding capacity. This decrease was not observed for D–MIP and may be related to limitations of the NIP in adsorbing and desorbing larger molecules such as proteins, possibly due to its morphology. However, it is important to mention that the material porosity alone does not justify the results related to the binding capacity, being the imprinting contribution mainly responsible for the MIP

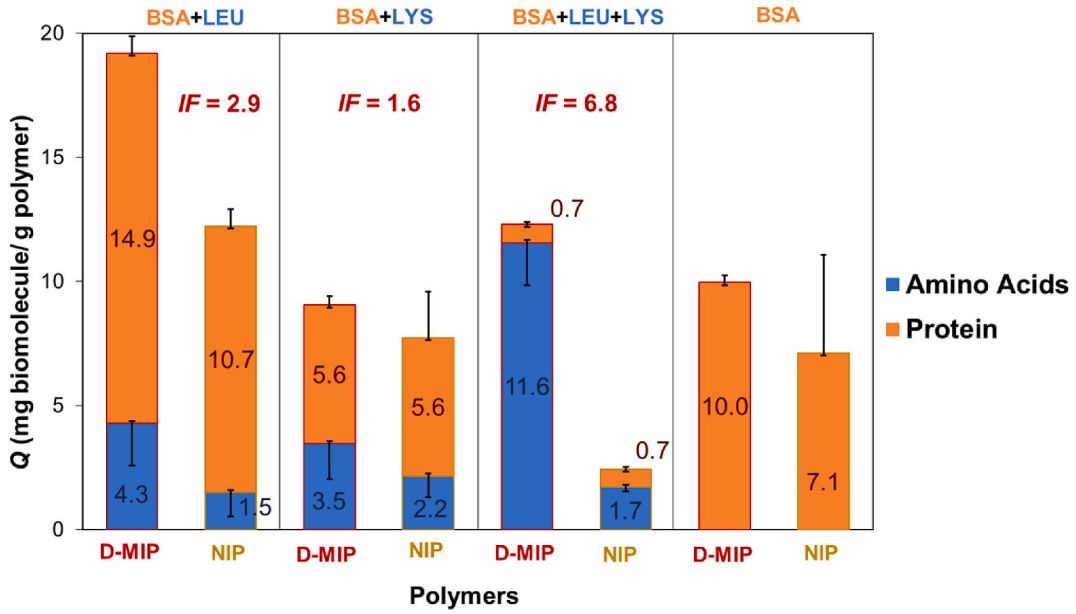

Fig. 8. SPE data of D–MIP and NIP using different amino acid + protein solutions: 0.25 mg BSA with 0.25 mg LEU, per mL; 0.25 mg BSA with 0.25 mg LYS, per mL; and 0.25 mg BSA with 0.125 mg LEU and 0.125 mg LYS, per mL; and just 0.25 mg BSA per mL. The *IF*s were calculated in terms of amino acid binding capacity.

binding capacity [11,36].

As previously indicated (Table 1), all the materials are neutral, with a zeta potential in the range ±10 mV, and only the NIP has a slightly negative surface charge [27]. All SBTs and SPE experiments were performed using aqueous solutions, and the pH of each solution was registered (Table S9 in Supplementary Information). Therefore, LEU is in a neutral form (pI = 5.98), while LYS (pI = 9.74), ARG (pI = 10.76) are positively charged. BSA is negatively charged (pI around 4.5–5.1), except for the mixed solution (BSA + LEU) where BSA could be in a neutral or even positively charged form [37,38]. Thereby, the favorable interaction's contribution due to the biomolecule's charges could be verified in the experiments with solutions containing LYS and ARG (solution with pH 12), especially for the control NIP. However, this contribution seems to be just relevant for the experiments using ARG in solution, for which higher binding capacities were obtained for NIP over D–MIPs (Fig. 7). On the other hand, the repulsion phenomena between BSA and the NIP surface could be justified by the low adsorption in most part of SPE experiments using the solutions containing the protein (Fig. 8), when compared the protein binding capacity to D–MIP [30]. As previously referred, this difference could also be related to the morphology of the polymers, with NIP exhibiting lower particle size, surface area, and pore volume compared to D–MIP.

Regarding the D–MIP results, interactions associated with the biomolecule charges and the polymer's surface charge seemed to have minimal impact on its binding performance, with the imprinting effect being the main determinant factor.

Looking to the charges of the molecules themselves, they revealed insights into the observed SPE–results. The opposite charges of the BSA and LYS might contribute to the lower binding capacities (in both amino acid and protein) obtained in the BSA + LYS assay, where the interaction between BSA and LYS might be favored over the interactions between the biomolecule and the polymer. Another example related to the molecule's charge can be observed in the BSA + LEU experiment (solution with pH 5), where BSA will have a charge almost positive facilitating the interaction between the BSA and the polymeric surface (mainly NIP), resulting in a higher protein binding capacity in the BSA + LEU solution compared to the BSA solution (pH 6). It is noted that even with empirical studies aimed at determining the charge of BSA at various pH levels, BSA is a macromolecule with a structure that exhibits regions with varying charges – some more positively charged and others negatively charged – showing the inherent complexity of the interactions behind the adsorption processes in aqueous media [38–40]. The complexity of protein–involved systems underscores the need for thorough comprehension, with further empirical and computational studies being essential to enhance our understanding on the interface interactions between polymeric surfaces and proteins, as well as elucidate the contribution of amino acids to these interactions.

In summary, this research work showed that in different media and processes (SBT *vs.* SPE) the D–MIP presented different binding performances in the adsorption of the template molecules, as shown in Table 3.

Table 3
Summary of the maximum binding capacity (Q_{max}) and corresponding imprinting factor (*IF*) obtained for each solution in the SPE experiments.

Test	Solution	Q_{max}	*IF*
SBT	LEU	163 mg LEU/g O–MIP	1.7
	LYS	193 mg LYS/g D–MIP	3.8
	LEU + LYS	216 mg LEU + LYS/g D–MIP	8.3
SPE	LEU	79 mg LEU/g D–MIP	1.6
	LYS	13 mg LYS/g O–MIP	1.4
	LEU + LYS	16 mg LEU + LYS/g D–MIP	1.3
	ARG	50 mg ARG/g O–MIP	1.0
	LEU + LYS + ARG	31 mg LEU + LYS + ARG/g D–MIP	1.5
	BSA + LEU	4.3 mg LEU/g D–MIP	2.9
	BSA + LYS	3.5 mg LYS/g D–MIP	1.6
	BSA + LEU + LYS	11.6 mg LEU + LYS/g D–MIP	6.8

As expected, binding capacities obtained by the SPE experiments were lower compared to those obtained in the SBTs, which might be due to the contact time between the material and the solution. Higher *IF*s were also obtained in the SBT when compared to the SPE experiments, mainly for the solutions containing LYS. In the presence of the flowrate (dynamic mode), the D–MIP microcavities were able to adsorb more easily the template molecule LEU that presents lower molecular volume in comparison to LYS, resulting better *IF*s in the solutions containing LEU.

In addition, in the SPE experiments using amino acid loading solutions, the D–MIP had better binding performance compared to the O–MIP. Finally, the D–MIP proved to have high affinity and selectivity for its template(s) amino acids even in solutions containing protein. Comparing the produced MIPs with the literature, similar binding performances, either on SBT or on SPE experiments, were obtained (*e.g., IF* = 1–3 for the target molecules) [21,41]. However, it should be highlighted the maximum values of *Q* and *IF* (Q_{max} = 216 mg amino acid/g D–MIP and IF_{max} = 8.3) from the D–MIP in the SBTs (Fig. 6) that are higher than the reported systems.

In a previous work from the literature, in accordance with our strategy, D–MIPs displayed higher molecular recognition ability and higher binding capacity in the SPE experiments [41]. In another system using a dual–template molecules similar in size to the one used in this work, though even larger than the amino acid, similar imprinting factor results were observed [42]. *Q* values were approximately 33 and 20 mg/g material in SBTs at 0.1 mg antibiotic/mL aqueous solutions, resulting in *IF*s of around 1.6 and 2.7. In our SBTs, despite using a solution with a higher biomolecule concentration (C_0 = 0.5 mg/mL), higher *Q* values were obtained (*Q* = 135 mg LEU/g D–MIP and 193 mg LYS/g D–MIP), with *IF*s of 1.3, 3.8 and 8.3. Additionally, when the green D–MIPs produced in this work are compared to the conventional MIPs developed for the same template molecules (LEU or LYS) at the aqueous solution concentration (C_0 = 0.5 mg/mL) and using a similar SBT protocol and amino acid quantification method, our work showed better binding performance (Table 4). For instance, the D–MIP for LYS outperformed the O–MIP reported by Panahi et al. (*Q* = 15 mg LYS/g MIP *vs.* 193 mg LYS/g D–MIP) [43], and exhibited higher *IF*s than the O–MIP for LYS from the study by Pisarev et al. (*IF* = 1.9 *vs.* our *IF*s of 3.8 and 8.3) [44]. For MIPs using LEU as the template and targeting the same molecule in SBTs despite a different amino acid quantification method (Table 4), our green D–MIP still showed higher *Q* values than the O–MIP reported (*Q* = 27 mg LEU/g MIP and *Q* = 18 mg LEU/g MIP *vs.* 135 mg LEU/g D–MIP in this study) [21].

These results emphasize the effectiveness of using $scCO_2$ as a green alternative for producing materials with high *IF*s, inclusive D–MIP with enhanced binding performance. Furthermore, the scalability of the process and the possibility of CO_2 recovery as solution to reduce the production costs of the MIPs highlight its potential for industrial applications (Table 4).

4. Conclusions

A dual–templating MIP targeting LEU and LYS (D–MIP) and a one–templating MIP targeting LEU (O–MIP) were successfully produced using $scCO_2$, despite the low solubility of the biomolecules in $scCO_2$. All

Table 4
Maximum binding capacity (Q_{max}) and corresponding imprinting factor (*IF*) obtained in this work *vs.* maximum binding capacity reported and corresponding *IF*, for 0.5 mg/mL concentration.

Solution	Q_{max} (mg/g D–MIP)	IF	Reported Q_{max} (mg/g MIP)	Reported *IF*	Ref.
LEU	135	1.3	27	12.1	[21]
LYS	193	3.8	15	37.5	[43]
			900	1.4	[44]

materials were obtained as white, free–flowing dry powders. In terms of static binding performance, the D–MIP showed similar performance to the O–MIP, with both MIPs clearly outperforming the non–imprinted material (NIP), resulting in imprinting factors ranging from 1.3 to 3.8. The maximum binding capacity achieved was 216 mg LYS + LEU/g for the D–MIP using a 0.5 mg/mL LYS + LEU aqueous solution. Given the potential of these materials as affinity–based stationary phases for bio-purification processes, solid–phase extraction (SPE) experiments were conducted with different loading solutions. The D–MIP exhibited the highest affinity and selectivity, with a maximum binding capacity of 79 mg LEU/g when exposed to a 0.5 mg/mL LEU solution. Notably, in SPE experiments with BSA + amino acid solutions, lower binding capacities were observed compared to those with individual amino acid solutions. The D–MIP also demonstrated excellent selectivity for its template molecules (amino acid vs. protein), achieving the highest imprinting factor of 6.8 for a 0.5 mg/mL BSA + LEU + LYS solution.

Herein a green and sustainable approach to produce D–MIPs is provided revealing significant dynamic binding capacity, even in more complex media (such as selectivity for their template–molecules in different biomolecules solutions). It also provides binding capacity data and valuable insights into the interactions between amino acids and MIPs, which are crucial for understanding their selective recognition in mixed biomolecule solutions. The findings highlight the ability of the D–MIP to selectively recognize its template molecules even in the presence of a protein, showcasing its potential for real–world applications in biopurification. Both MIPs were found to be attractive, low–cost, and sustainable solutions for obtaining tailor–made biorecognition materials, emphasizing their applicability as stationary phases in chromatographic techniques for biopurification processes within the biotechnology and biopharmaceutical industries.

CRediT authorship contribution statement

Ana I. Furtado: Writing – original draft, Validation, Methodology, Investigation, Conceptualization. **Diogo Lobato:** Writing – review & editing, Investigation. **Vasco D.B. Bonifácio:** Writing – review & editing, Validation, Supervision, Methodology, Conceptualization. **Raquel Viveiros:** Writing – review & editing, Validation, Supervision, Methodology, Investigation, Conceptualization. **Teresa Casimiro:** Writing – review & editing, Validation, Supervision, Methodology, Funding acquisition, Conceptualization.

Declaration of competing interest

The authors declare that they have no known competing financial interests or personal relationships that could have appeared to influence the work reported in this paper.

Acknowledgments

The authors would like to thank financial support from Fundação para a Ciência e a Tecnologia, Ministério da Ciência, Tecnologia e Ensino Superior (FCT/MCTES, Portugal), through projects PTDC/EQU–EQU/32473/2017, and PTDC/MEC–ONC/29327/2017. A.I.F. acknowledges her PhD grant (SFRH/BD/150696/2020) in the aim of the International Year of the Periodic Table – a Protocol established between the Portuguese Chemical Society (SPQ) and FCT/MCTES. R.V. would like to acknowledge for her Individual Support from Scientific Employment Stimulus (CEEC–IND, 2020.00377.CEECIND) from FCT/MCTES. The Associate Laboratory Research Unit for Green Chemistry – Clean Technologies and Processes – LAQV–REQUIMTE is financed by national funds from FCT/MCTES (10.54499/LA/P/0008/2020, 10.54499/UIDP/50006/2020, and 10.54499/UIDB/50006/2020).

Appendix A. Supplementary data

Supplementary data to this article can be found online at https://doi.org/10.1016/j.mtchem.2025.102586.

Data availability

Data will be made available on request.

References

[1] Biopharmaceutical bioseparation systems market to value $20bn. https://www.europeanpharmaceuticalreview.com/news/172719/biopharmaceutical–bioseparation–systems–market–to–value–20bn/. (Accessed 24 May 2024).
[2] A. Xue, S. Fan, Matrices and affinity ligands for antibody purification and corresponding applications in radiotherapy, Biomolecules 12 (821) (2022) 1–20, https://doi.org/10.3390/biom12060821.
[3] A.I. Freitas, L. Domingues, T.Q. Aguiar, Tag–mediated single–step purification and immobilization of recombinant proteins toward protein–engineered advanced materials, J. Adv. Res. 36 (2022) 249–264, https://doi.org/10.1016/j.jare.2021.06.010.
[4] C.K. Dixit, S. Bhakta, K.K. Reza, A. Kaushik, Exploring molecularly imprinted polymers as artificial antibodies for efficient diagnostics and commercialization: a critical overview, Hybrid Advances 1 (2022) 100001:1–10, doi:10.1016/j.hybadv.2022.100001.
[5] M. Teufl, C.U. Zajc, M.W. Traxlmayr, Engineering strategies to overcome the stability–function trade–off in proteins, ACS Synth. Biol. 11 (2022) 1030–1039, https://doi.org/10.1021/acssynbio.1c00512.
[6] O.I. Parisi, F. Francomano, M. Dattilo, F. Patitucci, S. Prete, F. Amone, F. Puoci, The evolution of molecular recognition: from antibodies to molecularly imprinted polymers (MIPs) as artificial counterpart, J. Funct. Biomater. 13 (12) (2022) 1–26, https://doi.org/10.3390/jfb13010012.
[7] Z. El–Schich, Y. Zhang, M. Feith, S. Beyer, L. Sternbæk, L. Ohlsson, M. Stollenwerk, A.G. Wingren, Molecularly imprinted polymers in biological applications, Biotechniques 69 (2020) 407–420, https://doi.org/10.2144/btn–2020–0091.
[8] R. Viveiros, S. Rebocho, T. Casimiro, Green strategies for molecularly imprinted polymer development, Polymers 10 (2018) 1–27, https://doi.org/10.3390/polym10030306.
[9] A.I. Furtado, R. Viveiros, T. Casimiro, MIP synthesis and processing using supercritical fluids, Methods Mol. Biol. 2359 (2021) 19–42, https://doi.org/10.1007/978–1–0716–1629–1_3.
[10] A.I. Furtado, V.D.B. Bonifácio, R. Viveiros, T. Casimiro, Design of molecularly imprinted polymers using supercritical carbon dioxide technology, Molecules 29 (926) (2024) 1–14, https://doi.org/10.3390/molecules29050926.
[11] N. Murdaya, A.L. Triadenda, D. Rahayu, A.N. Hasanah, A review: using multiple templates for molecular imprinted polymer: is it good? Polymers 14 (2022) 4441: 1–22, https://doi.org/10.3390/polym14204441.
[12] A. Abdipoor, A. Taheri, A. Rangin, New magnetic graphene oxide core–shell functionalized SBA–15 dual template imprinted polymer for μ–solid phase extraction of nortriptyline and amitriptyline in mice plasma, Sep. Purif. Technol. 298 (2022) 121615, https://doi.org/10.1016/j.seppur.2022.121615, 1-10.
[13] Z. Liu, Z.Z. Yin, G. Zheng, H. Zhang, M. Zhou, S. Li, Y. Kong, Dual–template molecularly imprinted electrochemical biosensor for IgG–IgM combined assay based on a dual–signal strategy, Bioelectrochemistry 148 (2022) 108267: 1–10, doi:10.1016/j.bioelechem.2022.108267.
[14] H. Hou, S. Tang, W. Wang, M. Liu, A. Liang, L. Sun, A. Luo, Electrochemical enantioanalysis of D– and L–cysteine with a dual–template molecularly imprinted sensor, J. Electrochem. Soc. 169 (2022) 037506:1–11, doi:10.1149/1945–7111/ac58c0.
[15] S. Han, A. Yao, Y. Ding, Q. Leng, F. Teng, L. Zhao, R. Sun, H. Bu, A dual–template imprinted polymer based on amino–functionalized zirconium–based metal–organic framework for delivery of doxorubicin and phycocyanin with synergistic anticancer effect, Eur. Polym. J. 170 (2022) 111161:1–10, doi:10.1016/j.eurpolymj.2022.111161.
[16] N. Surapong, Y. Santaladchaiyakit, R. Burakham, A water–compatible magnetic dual–template molecularly imprinted polymer fabricated from a ternary biobased deep eutectic solvent for the selective enrichment of organophosphorus in fruits and vegetables, Food Chem. 384 (2022) 132475:1–11, doi:10.1016/j.foodchem.2022.132475.
[17] R. Xing, Y. Wen, Y. Dong, Y. Wang, Q. Zhang, Z. Liu, Dual molecularly imprinted polymer–based plasmonic immunosandwich assay for the specific and sensitive detection of protein biomarkers, Anal. Chem. 91 (2019) 9993–10000, https://doi.org/10.1021/acs.analchem.9b01826.
[18] N.I. Wardani, P. Kanatharana, P. Thavarungkul, W. Limbut, Molecularly imprinted polymer dual electrochemical sensor for the one–step determination of albuminuria to creatinine ratio (ACR), Talanta 265 (2023) 124769:1–11, doi:10.1016/j.talanta.2023.124769.
[19] F. Beigmoradi, M. Rohani Moghadam, Z. Garkani–Nejad, A. Bazmandegan–Shamili, H.R. Masoodi, Dual–template imprinted polymer electrochemical sensor for simultaneous determination of malathion and carbendazim using graphene quantum dots, Anal. Methods 15 (2023) 5027–5037, https://doi.org/10.1039/d3ay01054f.

[20] Z. Du, Y. Li, C. Zeng, Y. Zhong, S. Wang, W. Liu, Q. Chen, M. Pang, Y. Wang, R. Zhu, H. Zhang, M. Zhu, Dual–template molecularly imprinted double emission proportional fluorescence sensor based on $CsPbBr_3$ and $CsPb(Br/I)_3$ perovskite quantum dots for visual, selective and sensitive detection of methyl eugenol and aristolochic acid A, Sensor. Actuator. B Chem. 417 (2024) 136189, https://doi.org/10.1016/j.snb.2024.136189, 1-12.
[21] A.I. Furtado, R. Viveiros, V.D.B. Bonifácio, A. Melo, T. Casimiro, Biomolecular fishing: design, green synthesis, and performance of L–leucine–molecularly imprinted polymers, ACS Omega 8 (2023) 9179–9186, https://doi.org/10.1021/acsomega.2c05714.
[22] H. Bouzid, C.M.C. Filho, J.R.C. Marques, A.J.M. Valente, L.M. Gando–Ferreira, A new approach on the amino acid lysine quantification by UV–visible spectrophotometry, Rev. Chem. 71 (2020) 159–175, https://doi.org/10.37358/rc.20.8.8290.
[23] K. Fila, Y. Bolbukh, M. Goliszek, B. Podkościelna, M. Gargol, B. Gawdzik, Synthesis and characterization of mesoporous polymeric microspheres of methacrylic derivatives of aromatic thiols, Adsorption 25 (2019) 429–442, https://doi.org/10.1007/s10450–019–00022–8.
[24] Molinspiration Cheminformatics, Molinspiration Cheminformatics Free Web Services, 2023.
[25] M.S. Da Silva, R. Viveiros, P.I. Morgado, A. Aguiar–Ricardo, I.J. Correia, T. Casimiro, Development of 2–(dimethylamino)ethyl methacrylate–based molecular recognition devices for controlled drug delivery using supercritical fluid technology, Int. J. Pharm. 416 (2011) 61–68, https://doi.org/10.1016/j.ijpharm.2011.06.004.
[26] L.M. Madikizela, S.S. Zunngu, N.Y. Mlunguza, N.T. Tavengwa, P.S. Mdluli, L. Chimuka, Application of molecularly imprinted polymer designed for the selective extraction of ketoprofen from wastewater, WaterSA 44 (2018) 406–418, https://doi.org/10.4314/wsa.v44I3.08.
[27] J.D. Clogston, A.K. Patri, Zeta potential measurement, Methods Mol. Biol. 697 (2011) 63–70, https://doi.org/10.1007/978–1–60327–198–1_6.
[28] N.B. Yacine, B. Hanane, Sample preparation techniques in biological and pharmaceutical sciences, Analytical Techniques in Biosciences: From Basics to Applications 2 (2022) 25–42, https://doi.org/10.1016/b978–0–12–822654–4.00010–5.
[29] D.S. Rajendran, A. Chidambaram, P.S. Kumar, S. Venkataraman, S. Muthusamy, D. V.N. Vo, G. Rangasamy, V.K. Vaithyanathan, V.K. Vaidyanathan, Three–phase partitioning for the separation of proteins, enzymes, biopolymers, oils and pigments: a review, Environ. Chem. Lett. 1 (2022) 1–24, https://doi.org/10.1007/s10311–022–01540–8.
[30] S. Mushtaq, M.A. Abbas, H. Nasir, A. Mahmood, M. Iqbal, H.A. Janjua, N. M. Ahmad, Probing the behavior and kinetic studies of amphiphilic acrylate copolymers with bovine serum albumin, Sci. Rep. 13 (2023) 1–13, https://doi.org/10.1038/s41598–023–27515–5.
[31] P. Szymaszek, P. Fiedor, A. Chachaj–Brekiesz, M. Tyszka–Czochara, T. Świergosz, J. Ortyl, Molecular interactions of bovine serum albumin (BSA) with pyridine derivatives as candidates for non–covalent protein probes: a spectroscopic investigation, J. Mol. Liq. 347 (2022) 118262:1–12, doi:10.1016/j.molliq.2021.118262.
[32] S. Çulha, C. Armutcu, L. Uzun, S. Şenel, A. Denizli, Synthesis of l–lysine imprinted cryogels for immunoglobulin G adsorption, Mater. Sci. Eng. C 52 (2015) 315–324, https://doi.org/10.1016/j.msec.2015.03.059.
[33] Y.N. Prajapati, B. Bhaduri, H.C. Joshi, A. Srivastava, N. Verma, Aqueous phase adsorption of different sized molecules on activated carbon fibers: effect of textural properties, Chemosphere 155 (2016) 62–69, https://doi.org/10.1016/j.chemosphere.2016.04.040.
[34] S. Ghosh, J. Dey, Interaction of bovine serum albumin with N–acyl amino acid based anionic surfactants: effect of head–group hydrophobicity, J. Colloid Interface Sci. 458 (2015) 284–292, https://doi.org/10.1016/j.jcis.2015.07.064.
[35] Q. Hou, R. Bourgeas, F. Pucci, M. Rooman, Computational analysis of the amino acid interactions that promote or decrease protein solubility, Sci. Rep. 8 (2018) 1–13, https://doi.org/10.1038/s41598–018–32988–w.
[36] A.N. Hasanah, N. Safitri, A. Zulfa, N. Neli, D. Rahayu, Factors affecting preparation of molecularly imprinted polymer and methods on finding template–monomer interaction as the key of selective properties of the materials, Molecules 26 (2021) 5612: 1–22, https://doi.org/10.3390/molecules26185612.
[37] V.S. Raghuwanshi, B. Yu, C. Browne, G. Garnier, Reversible pH responsive bovine serum albumin hydrogel sponge nanolayer, Front. Bioeng. Biotechnol. 8 (2020) 573: 1–10, doi:10.3389/fbioe.2020.00573.
[38] O. Adamczyk, M. Szota, K. Rakowski, M. Prochownik, D. Doveiko, Y. Chen, B. Jachimska, Bovine serum albumin as a platform for designing biologically active nanocarriers—experimental and computational studies, Int. J. Mol. Sci. 25 (2024) 37:1–19, doi:10.3390/ijms25010037.
[39] A.K. Srivastav, S.K. Gupta, U. Kumar, A molecular simulation approach towards the development of universal nanocarriers by studying the pH– and electrostatic–driven changes in the dynamic structure of albumin, RSC Adv. 10 (2020) 13451:1–9, doi:10.1039/d0ra00803f.
[40] A. Bujacz, Structures of Bovine, Equine and Leporine Serum Albumin, Acta Cryst 68 (2012) 1278–1289, https://doi.org/10.1107/s0907444912027047.
[41] C. Wang, C. Ding, Q. Wu, X. Xiong, Molecularly imprinted polymers with dual template and bifunctional monomers for selective and simultaneous solid–phase extraction and gas chromatographic determination of four plant growth regulators in plant–derived tissues and foods, Food Anal. Methods 12 (2019) 1160–1169, https://doi.org/10.1007/s12161–019–01455–1.
[42] W. Lu, J. Liu, J. Li, X. Wang, M. Lv, R. Cui, L. Chen, Dual–template molecularly imprinted polymers for dispersive solid–phase extraction of fluoroquinolones in water samples coupled with high performance liquid chromatography, Analyst 144 (2019) 1292–1302, https://doi.org/10.1039/c8an02133c.
[43] R. Panahi, E. Vasheghani–Farahani, S.A. Shojaosadati, Separation of L–lysine from dilute aqueous solution using molecular imprinting technique, Biochem. Eng. J. 35 (2007) 352–356, https://doi.org/10.1016/j.bej.2007.01.027.
[44] O.A. Pisarev, I.V. Polyakova, Molecularly imprinted polymers based on methacrylic acid and ethyleneglycol dimethacrylate for L–lysine recognition, React. Funct. Polym. 130 (2018) 98–110, https://doi.org/10.1016/j.reactfunctpolym.2018.06.002.